

# Water transport through subnanopores in the ultimate size limit: Mechanism from molecular dynamics

Jiyu Xu<sup>1,2,§</sup>, Chongqin Zhu<sup>3,§</sup>, Yifei Wang<sup>1,2,§</sup>, Hui Li<sup>1,4,§</sup>, Yongfeng Huang<sup>1,2</sup>, Yutian Shen<sup>1,2</sup>, Joseph S. Francisco<sup>3</sup>, Xiao Cheng Zeng<sup>3</sup> (✉), and Sheng Meng<sup>1,2</sup> (✉)

<sup>1</sup> Institute of Physics, Chinese Academy of Sciences, Beijing 100190, China

<sup>2</sup> School of Physical Sciences, University of Chinese Academy of Sciences, Beijing 100049, China

<sup>3</sup> Department of Chemistry, University of Nebraska, Lincoln, NE 68588, USA

<sup>4</sup> Beijing Advanced Innovation Center for Soft Matter Science and Engineering, Beijing University of Chemical Technology, Beijing 100029, China

<sup>§</sup> Jiyu Xu, Chongqin Zhu, Yifei Wang, and Hui Li contributed equally to this work.

© Tsinghua University Press and Springer-Verlag GmbH Germany, part of Springer Nature 2018

Received: 12 September 2018 / Revised: 2 November 2018 / Accepted: 26 November 2018

## ABSTRACT

*Ab initio* and classical molecular dynamics simulations show that water can flow through graphdiyne—an experimentally fabricated graphene-like membrane with highly dense ( $2.4 \times 10^{18}$  pores/m<sup>2</sup>), uniformly ordered, subnanometer pores (incircle diameter 0.57 nm and van der Waals area 0.06 nm<sup>2</sup>). Water transports through subnanopores via a chemical-reaction-like activated process. The activated water flow can be precisely controlled through fine adjustment of working temperature and pressure. In contrast to a linear dependence on pressure for conventional membranes, here pressure directly modulates the activation energy, leading to a nonlinear water flow as a function of pressure. Consequently, high flux (1.6 L/Day/cm<sup>2</sup>/MPa) with 100% salt rejection efficiency is achieved at reasonable temperatures and pressures, suggesting graphdiyne can serve as an excellent membrane for water desalination. We further show that to get through subnanopores water molecule must break redundant hydrogen bonds to form a two-hydrogen-bond transient structure. Our study unveils the principles and atomistic mechanism for water transport through pores in ultimate size limit, and offers new insights on water permeation through nanochannels, design of molecule sieving and nanofluidic manipulation.

## KEYWORDS

graphdiyne, subnanopore, molecular dynamics, water transport, desalination

## 1 Introduction

Understanding and controlling water transport through nanopores and nanochannels is of great importance to water desalination and purification [1–4], preservation of groundwater [5], design of biomimetic pores [6–9], and modulating biological cellular transport [10–12]. Low-dimensional graphene-like materials [13–19] and carbon nanotubes [20–24] show high water permeability. Dominated by the steric effect, water flow is linear with respect to the applied pressure and continuous through nanopores when van der Waals pore size is larger than  $\sim 0.2$  nm<sup>2</sup> [14, 17, 25, 26]. Molecular selectivity can be realized by tuning the size, shape and decoration of nanopores [16, 17, 27, 28], allowing water transport while preventing ion permeation. However, it is unclear what the ultimate size of nanopore is to allow transport of water molecules. The atomistic mechanism and working principles of water molecule entering subnanopores are also elusive [9]. Both issues are important for understanding water permeation through ultrasmall pores (e.g., zeolite and aquaporins) [12], design of molecule sieving [29], and nanofluidic manipulation [30–32].

Graphdiyne, a novel one-atom-thick carbon allotrope, has attracted considerable interests owing to its excellent mechanical, physical and electrochemical properties [33–37]. Uniform triangular nanopores with a van der Waals pore size of  $\sim 0.06$  nm<sup>2</sup> are periodically distributed in graphdiyne atomic plane (Fig. 1). Since the first fabrication of

large area graphdiyne films on copper foil via cross-coupling reactions [38], many synthesis methods have been explored [39–41]. Previous classical molecular dynamics (MD) simulations [17, 26] show that graphdiyne membrane is impermeable for water molecules. However, Bartolomei et al. [42] proposed a static analysis and posed the possibility of water permeation through graphdiyne, without considering the realistic structure of interfacial water. Therefore, graphdiyne can serve as an ideal membrane system for studying the critical pore size and the mechanism for water transport through ultrasmall nanopores. Recently, Yuan et al. [43] studied the mechanism of gas permeation through ultrasmall nanopores, where an energy barrier is found for the permeation of gas molecule in two steps: adsorption and translocation. The complex hydrogen-bonding network of water and interfacial molecular structure make the mechanism of water transport through ultrasmall nanopores even more intricate and delicate than gaseous molecules.

In this work, on basis of extensive *ab initio* molecular dynamics (AIMD) and classical molecular dynamics (CMD) simulations, we find that water flow through subnanometer pores of graphdiyne membrane is an activated process characterized by the Arrhenius equation. Contrary to conventional membranes, the rate of water flow through graphdiyne membrane is nonlinear with respect to the applied pressure, due to the modulation of activation energy by pressure. Large water flow with 100% salt rejection efficiency is achieved at reasonable pressures and temperatures, indicating

Address correspondence to Sheng Meng, smeng@iphy.ac.cn; Xiao Cheng Zeng, xzeng1@unl.edu

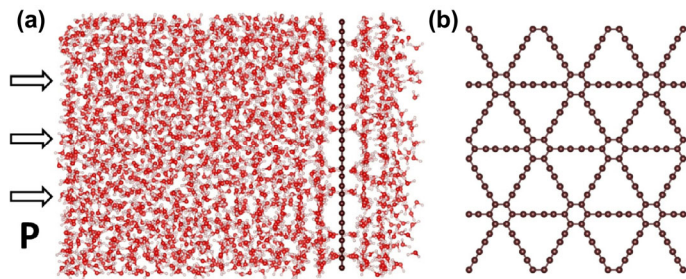


**Figure 1** (a) Side view of the system setup for MD simulations. (b) Atomic structure of the graphdiyne membrane. Color code: C, grey; O, red; H, white.

graphdiyne membrane is an excellent candidate for water purification and desalination applications. We also observe that water molecule must break redundant hydrogen bonds (HBs) with interfacial water and form a two-hydrogen-bond-structure as the transition state before water transport takes place. This work brings to bear effective ways to precisely control water transport through fine adjustment of working temperature and pressure, thanks to the newly found exponential dependence.

## 2 Computational methods

*Ab initio* MD simulations were performed with the CP2K package [44]. We chose the BLYP exchange-correlation functional [45, 46], the DZVP basis set and GTH pseudopotentials [47, 48]. The D3 empirical van der Waals corrections [49] were included to have reasonable description of water-water and water-membrane interactions. The AIMD simulations were performed in the *NVT* ensemble with a timestep of 1 fs. Nose-Hoover thermostat was used to control the temperature at 400 K,  $\sim 40$  K above the melting temperature of the BLYP-D ice (the melting temperature of bulk ice Ih predicted based on the BLYP-D functional is  $\sim 360$  K) [50]. The simulation system in *ab initio* MD simulations includes a hexagonal box with dimensions of  $9.8 \text{ \AA} \times 9.8 \text{ \AA} \times 40 \text{ \AA}$  with 44 and 18 water molecules located on feed and permeate sides of graphdiyne membrane initially (Fig. S1 in the Electronic Supplementary Material (ESM)). After structural optimization, five independent AIMD simulations were performed for 30–100 ps, for which the applied pressure applied on the graphene sheet (as the piston) ranges from 0.5 to 5 GPa.

Classical MD simulations were performed with the Gromacs 4.5.5 package [51]. The SPC/E water model was used [52]. Non-bonding interactions were modeled by Lennard-Jones potentials with the water-substrate interaction parameters  $\sigma_{C-O} = 3.02 \text{ \AA}$  and  $\epsilon_{C-O} = 1.734 \text{ kJ/mol}$ . The parameters reproduce nicely the energy barrier (185 meV) and the position of energy minimum obtained from DFT calculations for a water molecule passing through the subnanopore of graphdiyne membrane (see Fig. S2 in the ESM). The long-ranged electrostatic interactions were computed with particle-mesh Ewald summation method [53]. All classical MD simulations were performed with *NVT* ensemble and a timestep of 1 fs for 15 ns. The temperature was controlled by the Berendsen thermostat with target values ranging from 320 to 400 K [54]. The simulation system in classical MD simulations includes an orthogonal box with dimensions of  $39.2 \text{ \AA} \times 33.948 \text{ \AA} \times 300 \text{ \AA}$  with 2,145 and 395 water molecules initially located on feed and permeate sides, respectively, of the graphdiyne membrane (Fig. 1). The latter comprises 32 triangular nanopores. Desalination simulations were performed within the same supercell size by inserting 35  $\text{Na}^+$  and 35  $\text{Cl}^-$  in the feed side, which gives rise to the salinity  $S$  of about 50‰, slightly higher than that of 35‰ of seawater. The Amber99 force-field is used for both ions. The salt rejection is defined as

$$1 - \frac{S_{\text{permeate}}}{S_{\text{feed}}}. S_{\text{permeate}}$$
 is salinity of the permeate solution at the time

when half water molecules have flowed to the permeate side, and  $S_{\text{feed}}$  is the initial salinity of the feed.

## 3 Results and discussion

### 3.1 Water flow through graphdiyne membrane

In AIMD simulations, direct penetration of water molecules through the graphdiyne membrane was observed, confirming water permeability of the graphdiyne membrane. At pressure of 2 GPa and temperature of 400 K, water transport through graphdiyne membrane occurs within 100 ps. The corresponding water flow rate is  $0.012 \text{ ps/nm}^2$  (Fig. 2), namely,  $1.6 \text{ L/Day/cm}^2/\text{MPa}$ , two orders of magnitude higher than the commercial polymeric seawater reverse osmosis (RO) ( $0.01 \text{ L/Day/cm}^2/\text{MPa}$ ) [1, 2]. Surprisingly, at higher pressure of 5 GPa, water flow of  $10 \text{ L/Day/cm}^2/\text{MPa}$  can be achieved, which increases by another order of magnitude. Thus, water flow rate is nonlinearly dependent on the pressure applied to the piston. The unexpected nonlinear pressure dependence of water flux is dramatically different from previous studies, which all show a linear relationship to the applied pressure [17, 25, 26]. We note that the pore size in graphdiyne (effective incircle diameter:  $0.57 \text{ nm}$ ) is slightly less than two times of the size of a water molecule ( $0.31 \text{ nm}$ ). Thus, such a pore represents the ultimate size limit of subnanopores allowing effective water transport.

In view of the high computation cost of AIMD, we develop a more cost-effective approach to compute water flow rate without loss of accuracy. We employ CMD simulations with the parameters fitted to *ab initio* energy calculations. Compared with the unoptimized Amber99 force-field  $\sigma_{C-O} = 3.28279 \text{ \AA}$  and  $\epsilon_{C-O} = 0.48397 \text{ kJ/mol}$ , these parameters can reproduce the energy barrier of 185 meV and the position of potential energy minimum obtained from *ab initio* calculations, for a single water molecule passing through the graphdiyne membrane (see Fig. S2 in the ESM). As shown in Fig. 2, at 400 K, water flow rate obtained from CMD simulations is nearly the same as that from AIMD simulations.

The nonlinear dependence of water flow on pressure is confirmed in CMD simulations, and the water flow rate increases with temperature. At 340 K and 500 MPa, the water flow rate is  $0.1 \text{ L/Day/cm}^2/\text{MPa}$ , one order of magnitude higher than the commercial polymeric seawater RO. Furthermore, the nonlinear behavior leads to large water flux at relatively high pressure of 5 GPa, three orders of magnitude higher than that for commercial polymeric seawater RO. Although the pressure of 5 GPa considered is very high, water under this pressure still behaves like a liquid [55], while the graphdiyne membrane can sustain extreme uniaxial stress, as high as 40 GPa [17]. Though defects are unavoidable in realistic situations, previous studies demonstrate that the strength of  $\gamma$ -graphyne is only reduced by  $\sim 20\%$  with the introduction of vacancy defects [56, 57]. Besides,

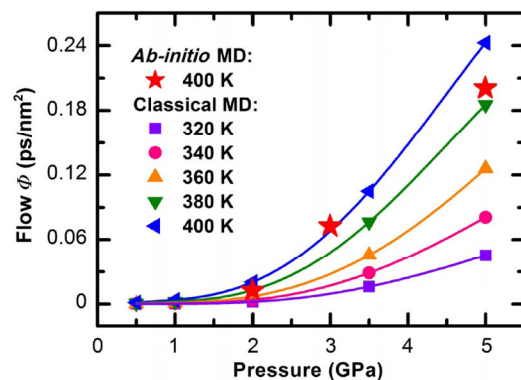


**Figure 2** Water flux versus the pressure and temperature in AIMD and CMD simulations. The solid line is the curve fitted to water flow rate in CMD simulations.

the rational design of porous supporting substrates that are widely used in the conventional reverse osmosis industry, would greatly enhance the mechanical strength of 2D materials, even for defective 2D materials [58]. We also note that the water flow in low pressure regions is greatly enhanced compared with that of the unoptimized parameters, owing to the accurate description of water-membrane interactions (Fig. S3 in the ESM). This accounts well for the reason why no water permeation was observed in previous studies [17, 26].

We also performed desalination simulations using a NaCl solution with salinity  $S$  of  $\sim 50\%$  as the feed side. Ions exist in the form of ion hydrates in aqueous solution, thus the dehydration effect dominates the transport of ions through ultimate-size nanopores. We simulate the desalination process with salty solutions, thus the effect of hydration shell of ions is explicitly included in the simulations. We find that the desalination efficiency of graphdiyne membrane is 100%, even at very high pressure of 5 GPa (Fig. S4 in the ESM). The superior salt rejection is attributed to three reasons. The first is that graphdiyne membrane are composed of inert carbon atoms, without bonding sites to facilitate the dehydration process as that in  $K^+$  channels [59]. The second is the effective pore size of  $0.06 \text{ nm}^2$ , smaller than that of  $0.1 \text{ nm}^2$  in MOF [60]. The third is that the electrical field used in previous works would only accelerate the charged ions and facilitate the dehydration process, while the hydrostatic pressure used here does not have such an effect. All these facts help to achieve a 100% salt rejection in graphdiyne even if the ion dehydration is explicitly considered.

We also note that water flow rate of single subnanopore (0.08 water molecules per ps) is of the same order as that of 0.8-nm-diameter narrow nanotubes ( $\sim 0.11$  water molecules per ps) [9]. Considering the ultrahigh pore density ( $2.4 \times 10^{18}$  pores/ $\text{m}^2$ ), graphdiyne membrane, the only sheet that has been experimentally synthesized in the graphyne family, shows a great potential in the realm of water purification and desalination technologies.

### 3.2 Activated water transport

Since water flux through graphdiyne is highly temperature dependent (see Fig. 2), we speculate that water transport is an activated process like that in typical chemical reactions. In other words, water molecules need to kinetically overcome a free energy barrier to pass through the subnanopores in graphdiyne membrane. As such, the flow flux would increase exponentially as temperature increases, following the Arrhenius equation

$$\phi = A_0 e^{-\frac{E_a}{kT}} \quad (1)$$

where  $\phi$  represents water flux,  $T$  the temperature,  $k$  the Boltzmann constant,  $A_0$  the prefactor corresponding to the trial frequency, and  $E_a$  the activation energy. Figure 3(a) shows the dependence of water flux on  $1/T$  in the logarithm scale. The excellent linear relationship indicates that the Arrhenius relationship can well account for the transport behavior of water molecules through graphdiyne subnanopores. The activation energy  $E_a$  decreases with pressure going from 410 meV at 500 MPa to 230 meV at 5 GPa, and nearly converges at high pressure region, implying the activation energy is modulated by pressure (Fig. 3(b)). The fitted prefactor  $A_0$  shows little changes, suggesting nearly the same topology structure of interfacial water. The  $E_a$  value of  $\sim 450$  meV at zero pressure also agrees well with the barrier ( $\sim 460$  meV) measured experimentally for water transport through 0.8-nm-diameter narrow nanotubes [9].

### 3.3 Atomistic mechanism

To gain deeper insights into the chemical-reaction-like temperature dependence for the water transport, we further explore atomistic mechanism of water flow through graphdiyne membrane. We track a typical trajectory of water molecule passing through graphdiyne

in AIMD simulations. Figures 4(a)–4(d) shows snapshots of a water molecule passing through the membrane in a chronological order, marked with arrows in Fig. 4(e). In the transport process, a water molecule is initially located right above the center of the triangular nanopore, forming about three HBs with water molecules on the same side of the membrane. An additional trans-membrane (TM) hydrogen bond with the water molecule on the other side of the membrane is also formed. Next, the water molecule breaks the redundant HBs until it has only one HB connecting water on each side of the membrane (Fig. 4(b)). With this unique two-hydrogen-bond transient structure, the water molecule is activated and the transport process proceeds. The two-hydrogen-bond structure holds throughout the transport process (Figs. 4(c) and 4(d)). Eventually, the water molecule moves to the bulk region on the other side of the membrane. In a word, water molecule must break its redundant HBs to allow for transport. The unique two-hydrogen-bond structure in the course of transport serves as the transition state for passing through the subnanopores of graphdiyne, implying water transport through subnanopores is intrinsically a many-body process in nature.

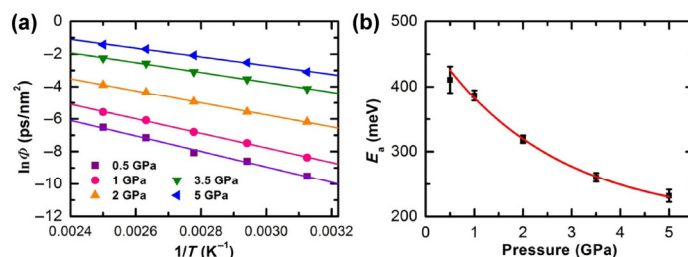


**Figure 3** (a) The dependence of water flux in logarithm scale on the inverse of temperature under different pressures. (b) The activation energy as a function of pressure.

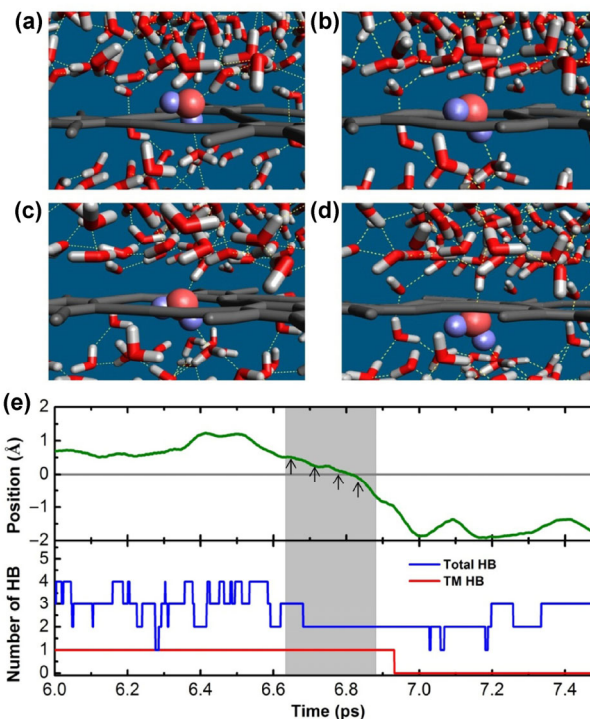


**Figure 4** (a)–(d) Snapshots of a water molecule transporting through graphdiyne subnanopores in chronological order. The transported water molecule is in spheric model, with oxygen in pink and hydrogens in purple, while other water molecules are in stick model with oxygens and hydrogens in red and white. Graphdiyne is shown in grey stick model. The HBs are illustrated with dashed white lines. (e) Position of the transported water molecule and the number of total HB and TM HB of the water molecule as a function of time. The shaded region indicates the time interval of water transport with four arrows indicating the time of four snapshots in (a)–(d).

The local structure of interfacial water fluctuates due to the presence of nanopores in graphdiyne membrane, giving rise to a distinct peak near the membrane in water density profile (see Fig. S5 in the ESM). It turns out that the location of the peak can serve as the activation sites for water transport. To see this point more clearly, we calculate the number of total HB and trans-membrane HB of water molecules at the activation sites at 340 K and at different pressure from the CMD simulations. As shown in Fig. 5(a), the number of total HB and TM HB is 3.7 and 1, respectively, regardless of the pressure, which implies its universality.

Water molecule at the activation site forms 3.7 HBs on average with interfacial water on both sides, namely, each water molecule has about four nearest neighbors, constituting a quasi-tetrahedron structure. Pressure does not affect the quasi-tetrahedron structure appreciably, although the peak corresponding to the activation sites shifts closer to the membrane as pressure increases (see Fig. 5(b)). The number of TM HB is 1, implying that the activation site is 100% occupied, and the TM HB always exists during the transport process. We note that the TM HB plays a key role in the emergence of the activation sites. Without the TM HB, the peak decreases greatly and shifts away from graphdiyne (Fig. S5 in the ESM). On average, 1.7 HBs are needed to break down during the transport of a water molecule through the membrane. The adsorption process for permeation of gas molecules [43] is absent for water transport in liquid state.

We also analyzed the orientation of OH group of water molecules at the activation sites in Fig. 5(c). The orientation angle is defined as the angle between the OH group and the surface normal direction (see inset of Fig. 5(c)). The peak slightly shifts to the left (smaller angle), due to the stronger compression at higher pressure. If both OH angles of a water molecule are greater than  $60^\circ$ , the water molecule acts as a TM HB acceptor. Otherwise, the water molecule is a TM HB donor. The integration below  $60^\circ$  gives rise to 25% at all pressures, suggesting that the proportion of two configurations (HB acceptor vs. donor) are equal and independent of pressure. Thus, whether water molecules act as the acceptor or donor of the TM HB does not affect water transport rate. This is consistent with

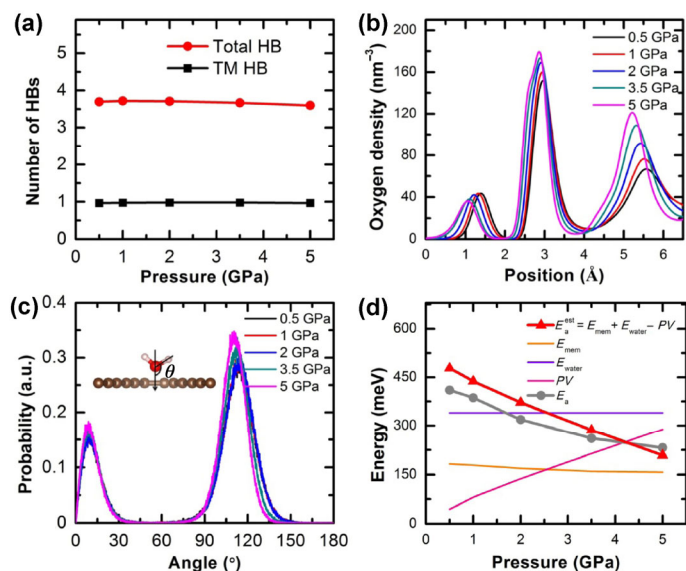


**Figure 5** (a) The average number of total HB and TM HB for the water molecule at the activation site as a function of pressure at 340 K. (b) The oxygen density profile along the direction perpendicular to graphdiyne membrane. (c) The orientation of OH bond of water molecules. The inset shows the definition of the OH orientation angle. (d) The estimated activation energy ( $E_a^{est}$ ), and its decomposition into that contributed by membrane ( $E_{mem}$ ), interfacial water molecules ( $E_{water}$ ), and pressure ( $PV$ ). For comparison, the activation energy from MD simulations ( $E_a$ ) is also shown.

the nearly same energy barrier for water transport in two different configurations (Fig. S2(c) in the ESM). This conclusion is contrary to the result from static calculations, as the realistic structure of interfacial water was not taken into account in the static calculations [42].

### 3.4 Origin of the activation energy

Based on the proposed atomistic mechanism and analysis of interfacial water structure shown above, the activation energy can be decomposed into three components in a rough estimation

$$E_a^{est} = E_{mem} + E_{water} - PV \quad (2)$$

where  $E_{mem}$  represents the energy barrier contributed by the graphdiyne membrane,  $E_{water}$  is the contribution by the HB interaction between the transported water and other interfacial water molecules,  $P$  is pressure, and  $V$  represents the effective volume of a water molecule. The  $PV$  term indicates the possibility of modulating activation energy by pressure. The activation sites shift closer to graphdiyne with increasing pressure, thus  $E_{mem}$  slightly decreases with pressure (Fig. 5(d)). About 1.7 HBs, independent of pressure, have to be broken during water transport. Thus,  $E_{water}$  is approximately  $1.7 \times 200 \text{ meV} = 340 \text{ meV}$  (assuming the average HB energy of 200 meV). We assume that  $V$  is the product of cross section area of water molecule and the distance of water molecule to membrane (Fig. S6 in the ESM). Then, we derive the numerical value of activation energy  $E_a^{est}$  according to Eq. (2).

As shown in Fig. 5(d), the activation energy estimated using Eq. (2) nicely coincides with the activation energy obtained from MD simulations. Therefore, the nonlinear dependence of water flux on pressure can be attributed to pressure-induced enthalpy change in the transition state. This conclusion suggests that the pressure can be used as a sensitive parameter to modulate the activation energy and, in turn, the water flux for membranes with the subnanopore size comparable to a single water. A dramatically enhanced water transport by orders of magnitude can be achieved by tuning up the pressure. We also note that the water flow regains the linear dependence on pressure in low pressure regions, which is demonstrated in the simulated water flow in low pressure regions (see Fig. S3 in the ESM), consistent with the expectations from Taylor's expansion of water flow at small pressures.

Our results are significantly different from previous studies [17, 26]. Based on conventional unoptimized force-fields, Xue et al. reported no water permeation through graphdiyne membrane in low pressure region. Despite the discussion on free energy barriers at constant temperature, the authors did not show the activation process for water transport with varying temperatures. In contrast, the nonlinear dependence of water flux on pressure in a wide range of pressures and the modulation on activation energy of activated water flow through the ultimate-sized nanopores in graphdiyne membrane are key findings of the present work. Besides, the activated flow allows for fine adjustment of flow rate by slightly raising the working temperature. At a slightly elevated temperature of 340 K, water flux with one order of magnitude higher rate than the commercial polymeric seawater RO, is obtained in low pressure regions. The thermal source can be the industrial waste heat, geothermal energy and solar thermal energy. In addition, the 100% salt rejection reduces the circular processing procedures and enhances the efficiency of industrial desalination. It endows graphdiyne membrane the potential to be integrated in high pressure desalination facility for the sake of both water permeability and selectivity. On the other hand, the modulation of activation energy by pressure gives insight to selective sieving of other species, e.g., separation of ions by electrical field. The two-hydrogen-bond transient state of water transport helps understanding water transport in MOF, minerals and biochannels, which motivates the design of biomimetic nanochannels.

## 4 Conclusions

In conclusion, on the basis of extensive AIMD and CMD simulations we show that water can flow through experimentally available graphdiyne membrane in an activated process described by the Arrhenius equation. The activated water flow can be precisely controlled through fine adjustment of working temperature and pressure. Meanwhile, the water flow rate exhibits nonlinear relationship with applied external pressure and large water flux can be achieved at high pressure with 100% salt rejection efficiency. Our results demonstrate that pressure is an effective means to modulate the activation energy and to drastically accelerate water transport through the ultimate-size pores. In nature water transport through subnanopores is a many-body process with the two-hydrogen-bond transient structure acting as the transition state. The new insights obtained from this study have far-reaching implications to the study of water permeation in minerals with subnanometer channels, and to the control of cellular water transport.

## Acknowledgements

We acknowledge financial support from Ministry of Science and Technology (No. 2016YFA0300902), the National Natural Science Foundation of China (Nos. 11474328 and 11290164) and Chinese Academy of Sciences (No. XDB070301).

**Electronic Supplementary Material:** Supplementary material (details of desalination simulations, energy profiles calculated with DFT and classical parameters, water flux in low pressure regions, density of interfacial water) is available in the online version of this article at <https://doi.org/10.1007/s12274-018-2258-7>.

## References

- Buelke, C.; Alshami, A.; Casler, J.; Lewis, J.; Al-Sayaghi, M.; Hickner, M. A. Graphene oxide membranes for enhancing water purification in terrestrial and space-born applications: State of the art. *Desalination* **2018**, *448*, 1138lin.
- Pendergast, M. M.; Hoek, E. M. V. A review of water treatment membrane nanotechnologies. *Energy Environ. Sci.* **2011**, *4*, 1946–1971.
- Shannon, M. A.; Bohn, P. W.; Elimelech, M.; Georgiadis, J. G.; Mariñas, B. J.; Mayes, A. M. Science and technology for water purification in the coming decades. *Nature* **2008**, *452*, 301–310.
- Elimelech, M.; Phillip, W. A. The future of seawater desalination: Energy, technology, and the environment. *Science* **2011**, *333*, 712–717.
- Post, V. E. A.; Groen, J.; Kooi, H.; Person, M.; Ge, S. M.; Edmunds, W. M. Offshore fresh groundwater reserves as a global phenomenon. *Nature* **2013**, *504*, 71–78.
- Yang, L. H.; Gordon, V. D.; Trinkle, D. R.; Schmidt, N. W.; Davis, M. A.; DeVries, C.; Som, A.; Cronan, J. E. Jr.; Tew, G. N.; Wong, G. C. L. Mechanism of a prototypical synthetic membrane-active antimicrobial: Efficient hole-punching via interaction with negative intrinsic curvature lipids. *Proc. Natl. Acad. Sci. USA* **2008**, *105*, 20595–20600.
- García-Fandiño, R.; Sansom, M. S. P. Designing biomimetic pores based on carbon nanotubes. *Proc. Natl. Acad. Sci. USA* **2012**, *109*, 6939–6944.
- Kosztin, I.; Schulten, K. Fluctuation-driven molecular transport through an asymmetric membrane channel. *Phys. Rev. Lett.* **2004**, *93*, 238102.
- Tunuguntla, R. H.; Henley, R. Y.; Yao, Y. C.; Pham, T. A.; Wanunu, M.; Noy, A. Enhanced water permeability and tunable ion selectivity in subnanometer carbon nanotube porins. *Science* **2017**, *357*, 792–796.
- Murata, K.; Mitsuoka, K.; Hirai, T.; Walz, T.; Agre, P.; Heymann, J. B.; Engel, A.; Fujiyoshi, Y. Structural determinants of water permeation through aquaporin-1. *Nature* **2000**, *407*, 599–605.
- Tajkhorshid, E.; Nollert, P.; Jensen, M. Ø.; Miercke, L. J. W.; O’connell, J.; Stroud, R. M.; Schulten, K. Control of the selectivity of the aquaporin water channel family by global orientational tuning. *Science* **2002**, *296*, 525–530.
- Horner, A.; Zocher, F.; Preiner, J.; Ollinger, N.; Siligan, C.; Akimov, S. A.; Pohl, P. The mobility of single-file water molecules is governed by the number of H-bonds they may form with channel-lining residues. *Sci. Adv.* **2015**, *1*, e1400083.
- Kidambi, P. R.; Boutilier, M. S. H.; Wang, L. D.; Jang, D.; Kim, J.; Karnik, R. Selective nanoscale mass transport across atomically thin single crystalline graphene membranes. *Adv. Mater.* **2017**, *29*, 1605896.
- Zhu, C. Q.; Li, H.; Meng, S. Transport behavior of water molecules through two-dimensional nanopores. *J. Chem. Phys.* **2014**, *141*, 18C528.
- Suk, M. E.; Aluru, N. R. Water transport through ultrathin graphene. *J. Phys. Chem. Lett.* **2010**, *1*, 1590–1594.
- Cohen-Tanugi, D.; Grossman, J. C. Water desalination across nanoporous graphene. *Nano Lett.* **2012**, *12*, 3602–3608.
- Zhu, C. Q.; Li, H.; Zeng, X. C.; Wang, E. G.; Meng, S. Quantized water transport: Ideal desalination through graphyne-4 membrane. *Sci. Rep.* **2013**, *3*, 3163.
- Kou, J. L.; Zhou, X. Y.; Lu, H. J.; Wu, F. M.; Fan, J. T. Graphyne as the membrane for water desalination. *Nanoscale* **2014**, *6*, 1865–1870.
- Lin, S. C.; Buehler, M. J. Mechanics and molecular filtration performance of graphyne nanoweb membranes for selective water purification. *Nanoscale* **2013**, *5*, 11801–11807.
- Holt, J. K.; Park, H. G.; Wang, Y. M.; Stadermann, M.; Artyukhin, A. B.; Grigoropoulos, C. P.; Noy, A.; Bakajin, O. Fast mass transport through sub-2-nanometer carbon nanotubes. *Science* **2006**, *312*, 1034–1037.
- Thomas, J. A.; McGaughey, A. J. H. Water flow in carbon nanotubes: Transition to subcontinuum transport. *Phys. Rev. Lett.* **2009**, *102*, 184502.
- Qin, X. C.; Yuan, Q. Z.; Zhao, Y. P.; Xie, S. B.; Liu, Z. F. Measurement of the rate of water translocation through carbon nanotubes. *Nano Lett.* **2011**, *11*, 2173–2177.
- Joseph, S.; Aluru, N. Why are carbon nanotubes fast transporters of water? *Nano Lett.* **2008**, *8*, 452–458.
- Striolo, A. The mechanism of water diffusion in narrow carbon nanotubes. *Nano Lett.* **2006**, *6*, 633–639.
- Wang, Y. J.; Li, L. B.; Wei, Y. Y.; Xue, J.; Chen, H.; Ding, L.; Caro, J.; Wang, H. H. Water transport with ultralow friction through partially exfoliated g-C<sub>3</sub>N<sub>4</sub> nanosheet membranes with self-supporting spacers. *Angew. Chem., Int. Ed.* **2017**, *56*, 8974–8980.
- Xue, M. M.; Qiu, H.; Guo, W. L. Exceptionally fast water desalination at complete salt rejection by pristine graphyne monolayers. *Nanotechnology* **2013**, *24*, 505720.
- Surwade, S. P.; Smirnov, S. N.; Vlassioug, I. V.; Unocic, R. R.; Veith, G. M.; Dai, S.; Mahurin, S. M. Water desalination using nanoporous single-layer graphene. *Nat. Nanotechnol.* **2015**, *10*, 459–464.
- Liu, J.; Shi, G. S.; Guo, P.; Yang, J. R.; Fang, H. P. Blockage of water flow in carbon nanotubes by ions due to interactions between cations and aromatic rings. *Phys. Rev. Lett.* **2015**, *115*, 164502.
- Han, J.; Fu, J. P.; Schoch, R. B. Molecular sieving using nanofilters: Past, present and future. *Lab Chip* **2008**, *8*, 23–33.
- Wan, R. Z.; Li, J. Y.; Lu, H. J.; Fang, H. P. Controllable water channel gating of nanometer dimensions. *J. Am. Chem. Soc.* **2005**, *127*, 7166–7170.
- Li, J. Y.; Gong, X. J.; Lu, H. J.; Li, D.; Fang, H. P.; Zhou, R. H. Electrostatic gating of a nanometer water channel. *Proc. Natl. Acad. Sci. USA* **2007**, *104*, 3687–3692.
- Gong, X. J.; Li, J. Y.; Zhang, H.; Wan, R. Z.; Lu, H. J.; Wang, S.; Fang, H. P. Enhancement of water permeation across a nanochannel by the structure outside the channel. *Phys. Rev. Lett.* **2008**, *101*, 257801.
- Li, Y. J.; Xu, L.; Liu, H. B.; Li, Y. L. Graphdiyne and graphyne: From theoretical predictions to practical construction. *Chem. Soc. Rev.* **2014**, *43*, 2572–2586.
- Zhang, S. L.; Liu, H. B.; Huang, C. S.; Cui, G. L.; Li, Y. L. Bulk graphdiyne powder applied for highly efficient lithium storage. *Chem. Commun.* **2015**, *51*, 1834–1837.
- Zhang, S. L.; Du, H. P.; He, J. J.; Huang, C. S.; Liu, H. B.; Cui, G. L.; Li, Y. L. Nitrogen-doped graphdiyne applied for lithium-ion storage. *ACS Appl. Mater. Interfaces* **2016**, *8*, 8467–8473.
- Wang, S.; Yi, L. X.; Halpert, J. E.; Lai, X. Y.; Liu, Y. Y.; Cao, H. B.; Yu, R. B.; Wang, D.; Li, Y. L. A novel and highly efficient photocatalyst based on P25-graphdiyne nanocomposite. *Small* **2012**, *8*, 265–271.
- Cranford, S. W.; Buehler, M. J. Selective hydrogen purification through graphdiyne under ambient temperature and pressure. *Nanoscale* **2012**, *4*, 4587–4593.
- Li, G. X.; Li, Y. L.; Liu, H. B.; Guo, Y. B.; Li, Y. J.; Zhu, D. B. Architecture of graphdiyne nanoscale films. *Chem. Commun.* **2010**, *46*, 3256–3258.

- [39] Qian, X. M.; Ning, Z. Y.; Li, Y. L.; Liu, H. B.; Ouyang, C. B.; Chen, Q.; Li, Y. J. Construction of graphdiyne nanowires with high-conductivity and mobility. *Dalton Trans.* **2012**, *41*, 730–733.
- [40] Matsuoka, R.; Sakamoto, R.; Hoshiko, K.; Sasaki, S.; Masunaga, H.; Nagashio, K.; Nishihara, H. Crystalline graphdiyne nanosheets produced at a gas/liquid or liquid/liquid interface. *J. Am. Chem. Soc.* **2017**, *139*, 3145–3152.
- [41] Gao, X.; Li, J.; Du, R.; Zhou, J. Y.; Huang, M. Y.; Liu, R.; Li, J.; Xie, Z. Q.; Wu, L. Z.; Liu, Z. F. et al. Direct synthesis of graphdiyne nanowalls on arbitrary substrates and its application for photoelectrochemical water splitting cell. *Adv. Mater.* **2017**, *29*, 1605308.
- [42] Bartolomei, M.; Carmona-Novillo, E.; Hernández, M. I.; Campos-Martínez, J.; Pirani, F.; Giorgi, G.; Yamashita, K. Penetration barrier of water through graphynes' pores: First-principles predictions and force field optimization. *J. Phys. Chem. Lett.* **2014**, *5*, 751–755.
- [43] Yuan, Z.; Govind Rajan, A.; Misra, R. P.; Draushuk, L. W.; Agrawal, K. V.; Strano, M. S.; Blankschtein, D. Mechanism and prediction of gas permeation through sub-nanometer graphene pores: Comparison of theory and simulation. *ACS Nano* **2017**, *11*, 7974–7987.
- [44] VandeVondele, J.; Krack, M.; Mohamed, F.; Parrinello, M.; Chassaing, T.; Hutter, J. Quickstep: Fast and accurate density functional calculations using a mixed gaussian and plane waves approach. *Comput. Phys. Commun.* **2005**, *167*, 103–128.
- [45] Becke, A. D. Density-functional exchange-energy approximation with correct asymptotic behavior. *Phys. Rev. A* **1988**, *38*, 3098–3100.
- [46] Lee, C.; Yang, W. T.; Parr, R. G. Development of the Colle-Salvetti correlation-energy formula into a functional of the electron density. *Phys. Rev. B* **1988**, *37*, 785–789.
- [47] Goedecker, S.; Teter, M.; Hutter, J. Separable dual-space Gaussian pseudopotentials. *Phys. Rev. B* **1996**, *54*, 1703–1710.
- [48] Hartwigsen, C.; Goedecker, S.; Hutter, J. Relativistic separable dual-space Gaussian pseudopotentials from H to Rn. *Phys. Rev. B* **1998**, *58*, 3641–3662.
- [49] Grimme, S.; Antony, J.; Ehrlich, S.; Krieg, H. A consistent and accurate *ab initio* parametrization of density functional dispersion correction (DFT-D) for the 94 elements H–Pu. *J. Chem. Phys.* **2010**, *132*, 154104.
- [50] Yoo, S.; Xantheas, S. S. Communication: The effect of dispersion corrections on the melting temperature of liquid water. *J. Chem. Phys.* **2011**, *134*, 121105.
- [51] Pronk, S.; Páll, S.; Schulz, R.; Larsson, P.; Bjelkmar, P.; Apostolov, R.; Shirts, M. R.; Smith, J. C.; Kasson, P. M.; van der Spoel, D. et al. GROMACS 4.5: A high-throughput and highly parallel open source molecular simulation toolkit. *Bioinformatics* **2013**, *29*, 845–854.
- [52] Berendsen, H. J. C.; Grigera, J. R.; Straatsma, T. P. The missing term in effective pair potentials. *J. Phys. Chem.* **1987**, *91*, 6269–6271.
- [53] Darden, T.; York, D.; Pedersen, L. Particle mesh ewald: An  $N \cdot \log(N)$  method for ewald sums in large systems. *J. Chem. Phys.* **1993**, *98*, 10089–10092.
- [54] Berendsen, H. J. C.; Postma, J. P. M.; van Gunsteren, W. F.; DiNola, A.; Haak, J. R. Molecular dynamics with coupling to an external bath. *J. Chem. Phys.* **1984**, *81*, 3684–3690.
- [55] Sanz, E.; Vega, C.; Abascal, J. L. F.; MacDowell, L. G. Phase diagram of water from computer simulation. *Phys. Rev. Lett.* **2004**, *92*, 255701.
- [56] Li, M. Y.; Zhang, Y. M.; Jiang, Y. L.; Zhang, Y.; Wang, Y. M.; Zhou, H. M. Mechanical properties of  $\gamma$ -graphyne nanotubes. *RSC Adv.* **2018**, *8*, 15659–15666.
- [57] Ajori, S.; Ansari, R.; Mirnezhad, M. Mechanical properties of defective  $\gamma$ -graphyne using molecular dynamics simulations. *Mater. Sci. Eng.: A* **2013**, *561*, 34–39.
- [58] Cohen-Tanugi, D.; Grossman, J. C. Mechanical strength of nanoporous graphene as a desalination membrane. *Nano Lett.* **2014**, *14*, 6171–6178.
- [59] Kopec, W.; Köpfer, D. A.; Vickery, O. N.; Bondarenko, A. S.; Jansen, T. L. C.; de Groot, B. L.; Zachariae, U. Direct knock-on of desolvated ions governs strict ion selectivity in  $K^+$  channels. *Nat. Chem.* **2018**, *10*, 813–820.
- [60] Zhang, H. C.; Hou, J.; Hu, Y. X.; Wang, P. Y.; Ou, R. W.; Jiang, L.; Liu, J. Z.; Freeman, B. D.; Hill, A. J.; Wang, H. T. Ultrafast selective transport of alkali metal ions in metal organic frameworks with subnanometer pores. *Sci. Adv.* **2018**, *4*, eaaq0066.